LiDAR Assisted Camera Inspection of Wind Turbines

Experimental Study

Durdevic, Petar; Ortiz Arroyo, Daniel; Yang, Zhenyu

Published in:
Proceedings of 2019 1st International Conference on Electrical, Control and Instrumentation Engineering (ICECIE)

DOI (link to publication from Publisher):
10.1109/ICECIE47765.2019.8974795

Publication date:
2019

Document Version
Accepted author manuscript, peer reviewed version

LiDAR Assisted Camera Inspection of Wind Turbines: Experimental Study

1st Petar Durdevic
Department of Energy Technology
Aalborg University
Esbjerg, Denmark
pdl@et.aau.dk

2nd Daniel Ortiz-Arroyo
Department of Energy Technology
Aalborg University
Esbjerg, Denmark
doa@et.aau.dk

3rd Zhenyu Yang
Department of Energy Technology
Aalborg University
Esbjerg, Denmark
yang@et.aau.dk

***Abstract*—In the fight against global climate change, the number of wind turbines installed globally is increasing. These complex structures need continuous inspection to asses their state and to repair them if needed. For this reason, wind turbine inspection activities have increased globally. This work proposes a method for how to improve the quality of data produced by visual unmanned aerial vehicles in wind turbine inspections. To accomplish this task, a multi-beam LiDAR is used in combination with an RGB camera. The LiDAR measures the distance from the camera to the wind turbine accurately. Additionally, the size of possible damages on the structure of the wind turbine are estimated, which is a valuable information to asses potential structural damages that may affect the long term productive life-cycle of a wind turbine.**

***Index Terms*—Drones, LiDAR, multi-beam solid state LiDAR, Inspection, Camera, Modeling, Wind Turbines**

I. Introduction

The global demand for renewable energy is growing due to the impact that the massive use of fossil fuels have on the environment. One of the leading technologies is the production of energy generated by wind turbines. Current state of the art wind turbines are very large structures having a blade diameter of 190 meters that is expected to grow in the coming years [1]–[3]. Such large structures are often placed in harsh environments that put an additional strain, leading eventually to produce failures in the structure [4].

A modern wind turbine has an expected lifetime of 20-25 years, with the manufacturing materials accounting for 70 to 80% of its environmental impact, [3]. [3] shows that proper recycling of materials at the end-of-service-life has a huge economical and environmental benefit. However, prolonging the lifetime of the structures performing regular inspections has a high importance as well. In this respect, unmanned aerial vehicles (UAVs) can be used to check regularly the wind turbines, improving its maintenance.

The number of aerial inspections of wind turbine installations is growing globally as this technology improves inspection quality in comparison to the use of conventional operator based inspections.

Most UAV-based inspections are performed by an operator that manually controls a drone's flight. Operators fly the drones at a safe distance from the inspection object, capturing images alongside the wind turbine structures and blades. These images are later analyzed by human inspectors, who visually detect faults and damages. Although software for automated computer vision-based detection of failures may be also used [4], [5] for this purpose. Additionally, autonomous AI-based systems are also emerging [6], to free the operator of the burden of operating a drone.

The quality of the inspection, whether it is done by a human or a machine, depends on many factors, such as image quality, lighting conditions, sharpness of images, and information about fault sizes, among others. The output of wind turbine inspections is a collection of images that include the approximate location and size of the fault, the extent of the damage and the type of damage, e.g. lighting strike, rain erosion, etc.. However, an important factor missed in most inspection reports is determining the position and size of the damage on a wind turbine. This information can help inspectors and operators of a specific wind turbine to asses damages's severity so that a proper plan could be designed for repairing these faults.

One of the challenges that wind turbine inspectors face when collecting images, is how to associate the images to the specific place on the structure where they were taken. This issue comprises several tasks:

- Location of the detected fault
- Determining the size of the damage

The size of a damage may be estimated in relation to wind turbine structure size. However, when damages are small hairline cracks, these estimates will be imprecise.

The literature on drone-based inspections is extensive. In [7] the performance of a system that combines radio-graphic and ultrasonic techniques to detect different properties of defects is described. The system tested was capable of detecting defects with sizes in the range of millimeters. This technique, although very precise, has only been tested in a controlled laboratory environment. UAVs and drones were used in [5], [8], [9], to take photos of damages in wind-turbines and analyze them using a variety of techniques, but without accounting for the exact size of the damaged area.

[4] discusses a method where faults are first manually extracted from images. Then, wavelet transforms are applied

This work has been supported by Department of Energy Technology at Aalborg University and Aerodyne AtSite A/S.

to these images to extract Haar-like features. These features are used to train an extended cascading classifier that is capable of detecting faults in images with different lighting conditions. Results show that the classifier is capable of detecting cracks larger than 10×40 pixels in length and width, but the paper does not mention how the actual size of the cracks are determined. In [8] wind turbine blades are inspected using active infrared thermography. Results obtained by the application of this method showed that it can be very effective, since it was able to detect 100% of the faults in the experiments performed. However, even though the paper shows the size of some of the faults with respect to the size of the blade, the authors do not discuss how this can be measured automatically from the thermographic data they collected. In [9], an UAV for automatically performing inspection flights on wind turbines is proposed using a 3D mapping of the wind turbine, spline-based path planning, collision avoidance and a distance control system. A 2D LiDAR is used to create a 3D map of the wind turbine and inspections are performed using the spline-based path planning algorithm. A UAV is also used in [5] to asses the potential damages in buildings and other structures using computer vision techniques.

In all the aforementioned works, the problem of assessing the actual size of the damaged area is not discussed. For instance, although a valid method is described in [10], using a LiDAR as a reference against which in-flight camera calibration can be performed, no measurements are reported. The method used to align a set of photogrammetric points to the LiDAR reference surface is the least squares algorithm. This method was used in aerial surveying of terrains.

LiDARs have been also used to create topographic maps and identify faults in seismic areas from Airborne point-cloud data in [11], showing good results.

These methods are related to the work presented in this paper, but they deal with problems at a larger scale and therefore, they not directly applicable for wind turbine damage detection.

Using a different approach, [12] combines a camera and an ultrasonic sensor mounted on a ground robot to detect simple objects and measure its size. First the distance from the robot's camera to the object is measured. Then, this data is used to calculate object's size from the width size of the view field in the camera. The precision obtained by this simple system was from 3.2 to 20.6% of accuracy, measured in centimeters. However, due to the inherent imprecision of ultrasonic transducers and its low resolution, these sensors are not suitable to use in wind turbine inspections.

The aim of this paper is to propose a method for enhancing the quality of wind turbine inspections and its posterior image analysis. The goal is to enriching the information acquired by the drone's RGB camera through precise depth measurements, using a LiDAR. We used a multi-beam LiDAR instead of a single-beam LiDAR, to increase the likelihood of producing a measurement and to get multiple measurements from a single image. The benefits of using a multi-beam LiDAR to detect the size of faults within the surface of a wind turbine is discussed.

In this work a prototype has been designed, built and experimentally evaluated in a real life scenario. A pinhole camera model is used to estimate the image pixel size, and through pixel counting the sizes of objects can be estimated. Using our method, photographs taken by an UAV of a wind turbine were used to estimate the size of several features with relatively high precision.

The main limitation of our study is the resolution of the LiDAR used. With the current Lidar is not possible to measure important parts of a wind turbine structure, such as wing tips and trailing edges.

II. Experimental Setup

A stand alone prototype was designed for this work, consisting of a multi-beam LiDAR module suspended in a gimball mount (DJI Ronin) attached to the underside of an UAV, in our case a Hexacopter (DJI Matrice 600). This ensured that the instruments are kept perpendicular to the horizon.

The images are captured by a Sony a7R II, with a sensor resolution of 7952×5304, and a physical size of 35.9mm $\times$ 23.9mm, i.e. a full frame sensor, which relates to a pixel size of $7950/23.9 = 0.0045$mm. The focal length of the lens is 50 mm. The FOV of the camera is $39.5°$. The LiDAR is a Leddar VU8, 8 segment LiDAR with horizontal $48°$ FOV, and $3°$ vertical FOV. The LiDAR used in this work is produced by LEDDAR tech and it is a Flash Solid-State LiDAR, with no moving components, which makes it suitable for UAV applications. The LiDAR offers simultaneous measurements from the 8 segments with up to 100 Hz [13]. The camera's shutter signal triggers an interrupt that enables LiDAR's reading function. This ensures that the LiDAR data is aligned with the images. The data is continuously stored onto a SD card, and the images and the LiDAR data are merged post flight. The software that performs all these operations runs on an Atmel SAM3X8E MCU.

III. Method

This section introduces the methods devised for measuring the distance from the camera to the object, and its application for image pixel size gauging.

A. Camera to Object Distance

The LiDAR outputs periodically an angle θ and a distance l_l. For each sample the LiDAR outputs a vector shown in equation 1.

$$L = \begin{bmatrix} [l_{l_1}, \ldots, l_{l_N}] \\ [\theta_1, \ldots, \theta_N] \end{bmatrix} \tag{1}$$

Where N is the amount of sequential beams that the LiDAR emits and receives. In our case $N = 8$, with a $\Delta\theta = 6°$ adding to a total field of view (FOV) of up to $48°$. From the LiDAR measurements, eight locations in a Cartesian coordinate system can be computed using the LiDAR Beam model shown in equation 2.

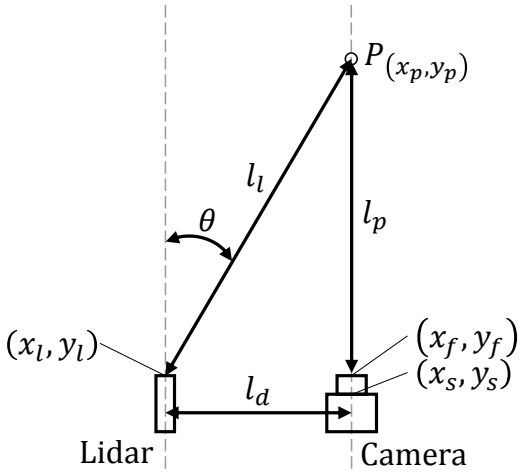

Fig. 1. Sketch of the Lidar and Camera setup.

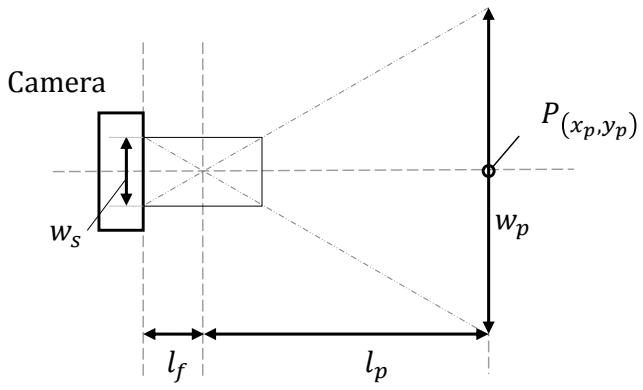

Fig. 2. Sketch of the pinhole camera.

$$[x_p^n, y_p^n]^T = l_l \begin{bmatrix} sin(\theta_n) \\ cos(\theta_n) \end{bmatrix} \tag{2}$$

The beam of the LiDAR is emitted and received at point $[x_l, y_l]$, thus the distance l_l will be the euclidean distance from the measured point and the point of LiDAR's emission as shown in equation 3, [14].

$$l_l = \sqrt{(x_p - x_l)^2 + (y_p - y_l)^2} \tag{3}$$

The angle of measurement can be found using the two points in space as shown in equation 4

$$\theta_n = atan2(y_p - y_l, x_p - x_l) \tag{4}$$

As figure 1 shows, the LiDAR and the camera are placed shifted in the x direction by a length of l_d. The origin of the camera with respect to the LiDAR will be $x_s = x_l + l_d$. This is crucial to referencing the points x_p that the LiDAR has detected as the points in the image.

B. Object Size Estimation

Our method is based on a pinhole camera model, where the camera consists of two main elements, an image sensor with width w_s and a lens with a focal length l_f, as illustrated in figure 2. If these parameters are constant, then the width of the FOV, w_p, at any given point P can be estimated, if the distance l_p to the point P is known. This also means that w_p is relative, and proportional to l_p. The consequence of this, is that w_p corresponds to a single point P in the FOV. If the point is part of a flat plane, then w_p can be calculated based on the distance l_p from the camera to the point P.

For an arbitrary point P, corresponding to the location of some unknown object, the measurement l_p is acquired by the LiDAR and the width of the object plane w_p, can be found using a perspective projection, as illustrated by equations 5, 6 and 7, [15].

$$l_p = x_p - x_f \tag{5}$$

$$w_p = \frac{l_p}{l_f} \cdot w_s \tag{6}$$

$$\frac{w_p}{w_{pixel}} = g[mm/pixel] \tag{7}$$

where w_{pixel} is the horizontal pixel count of the camera frame, w_s is the horizontal width of the sensor and g is the relative width at the object relative to the sensor pixel. By counting the number of pixels in the image, the object's size can be computed. This method can be used for an arbitrary point in the image, as long as the length measurement l_p to the x_p coordinate is available.

C. Data Quality

Although a LiDAR has high accuracy in measuring distances compared to other sensors, its data is subjected to measurement errors, such as: noise, failures and measurement of unexpected objects. In this work the data was not preprocessed but directly collected from the LiDAR.

The LiDAR was tested in a laboratory setting to evaluate its performance. An initial test was performed with the LiDAR facing a white wall at a fixed distance of 710 cm, collecting distance measurements at 10Hz for a period of 315 seconds. A histogram, shown in figure 3, represents the measurements of the 8 individual beams. As it can be expected, the distances measured increase, the further from the center of the light beam they are performed. As expected, the quality of the data collected in this experiment is exceptional. We measured a small standard deviation below 0.5 cm for the center beam and a maximal standard deviation of 0.87 for beam 1, which complies with the 1cm resolution stated in the specification of the instrument.

Figure 4 shows a histogram of data collected by flying the drone on a wind turbine. From this plot we can observe that the data collected from the outer four LiDAR's beams: $[l_1, l_2, l_7, l_8]$, is zero with relatively high frequency. This

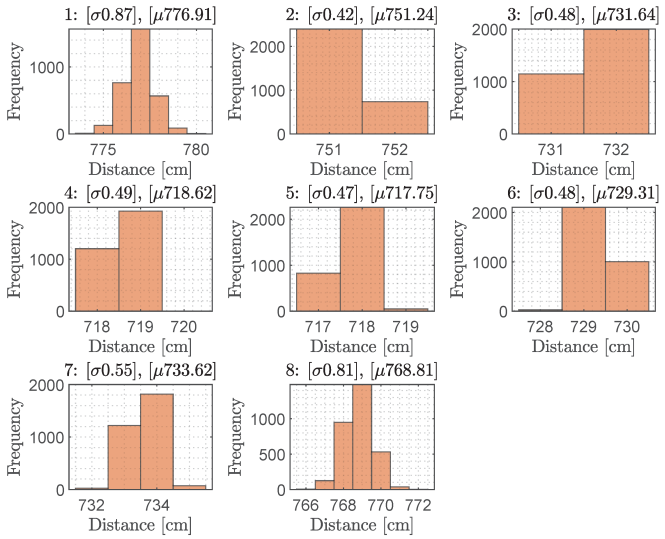

Fig. 3. Distance data from each LiDAR beam when tested facing a white wall.

is caused by measurement failures, which occurs when the LiDAR does not detect any object. As the LiDAR used in this work has a larger field of view than the camera, the measurements performed further away from the center beam produce maximum readings. The maximum reading ranges specified by the manufacturer are 85, 19, 13 meters for a retro reflector, white target, and gray target respectively.

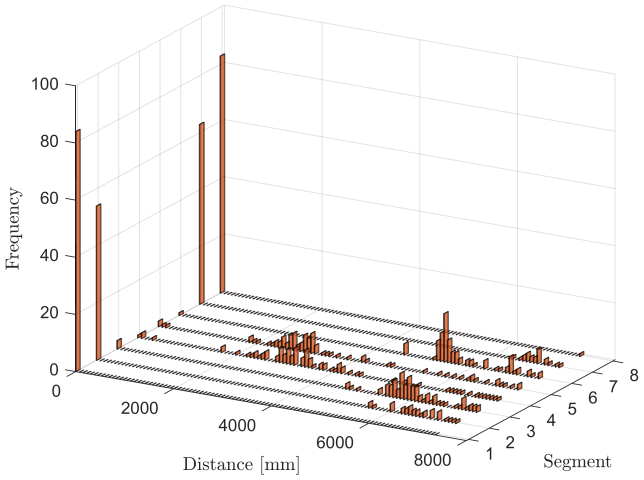

Fig. 4. Histogram representing each of the eight LiDAR beams, data streams from the experiment shown in figure 5

IV. Results

Two experiments were performed in this work. The main experiment, **Tower Inspection**, consisted in making the drone to ascend vertically alongside a wind turbine tower. The data collected from this experiment is the main result produced by this work. The second experiment, **Blade Inspection**, was performed by making the drone ascend vertically, from the wind turbine hub along the blade and until the blade tip was reached. During both experiments, the turbine was kept in a static position and the blades were initially pitched into the feathered position. The tests were performed on a Bonus B1300 wind turbine, S4 K2 "with B29 wings" (30m length), the wind turbine is located near Billund, Denmark.

A. Tower Inspection

The experiment was performed by flying the UAV from the bottom of the wind turbine to the hub, with an ascending velocity of approximately 1m/s. Images from the wind turbine were captured every second. The collected data is plotted in figure 5, showing the profile of the wind turbine.

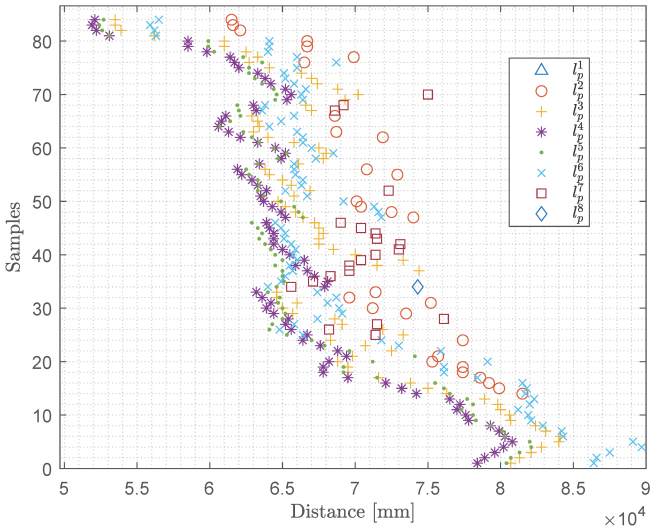

Fig. 5. Distance data collected during the experiment.

To evaluate the accuracy of our method, objects of known sizes were identified at first. For this purpose, the door and the door handle at the bottom of the tower were chosen. Figure 6 shows the image taken for the first inspection task, where the door dimensions were manually measured to be 2070×690mm (height × width) and the width of the handle was measured as 190mm.

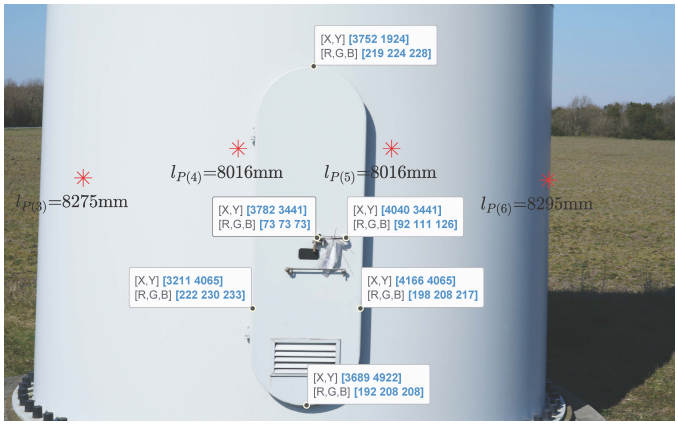

Fig. 6. Photo of wind turbine's door located on the base of the tower.

The two locations that are nearest to the door and with distance measures of 8016mm were used for the calculation. Using equation 6 and 7 we get the following ratio:

$$ratio = \frac{l_p}{l_f} \cdot \frac{ws}{w_{pixel}} = \frac{8016}{50} \cdot \frac{35}{7952} = 0.72 \frac{mm}{pixel} \quad (8)$$

Counting the number of pixels for the door and multiplying it with the previous ratio, the door's width and height are calculated as 2169.89×691.21mm and the width of the handle is calculated as 186.73mm. This results produce an error estimation for the door's width and height of 4.60% and 0.17% and for the handle's width -1.75%. These results show that our method can be used to measure with an acceptable precision some of the features of a wind turbine.

B. Tower Inspection 2nd Part

Since the method has been shown to perform well, we tested it with a photo of a small rust spot, located between point 3 and 4 and marked by an arrow in figure 7.

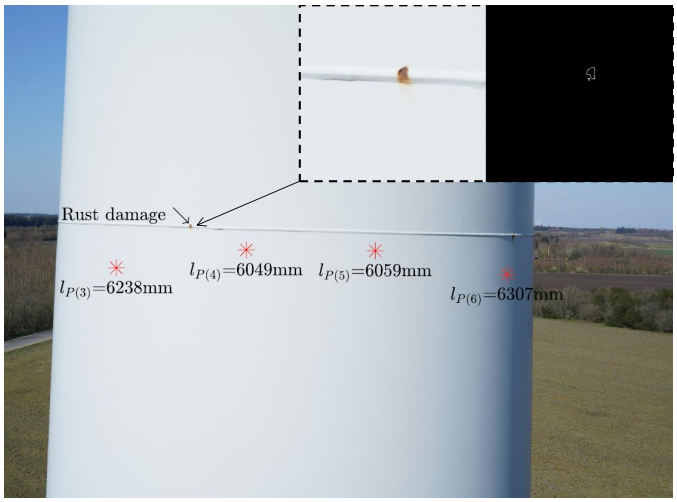

Fig. 7. Photo with detected points, image corresponds to sample 64 in figure 5.

Due to LiDAR's resolution, the distance will be estimated assuming that the wind turbine has approximately a flat surface. Using our method we estimate the distance of the rust spot from the drone to be approximately 6157.2mm. However, it should be noted that given that the shape of the tower is known, the exact distance could be calculated using trigonometry but this approach in general cannot be applied for more complex shapes such as the blades.

Given that the focus of this paper is not about the accurate detection and quantification of faults, we used traditional computer vision techniques to compute the size of the damaged area in the rust spot. First, we manually identified the rust damage by visually inspecting all images. Then, a Sobel filter is used to isolate the rust affected area from the white surface. This is shown in the top right of figure 7. Next, the Moore-Neighbor tracing algorithm is used together with the Jacob's stopping criteria, to trace the contour of the damaged area. The pixel density within the contour is then computed as was done in [16]. Using this method, the total area of the rust spot has been estimated to 367 pixels. Using equation 6 and 7 the area of each pixel can be found.

$$ratio = \frac{l_p}{l_f} \cdot \frac{ws}{w_{pixel}} = \frac{6157.2}{50} \cdot \frac{35}{7952} = 0.56 \frac{mm}{pixel} \quad (9)$$

thus the area of the rust spot is

$$pixel \cdot ratio = 367 \cdot 0.56 = 204.03 mm^2 \quad (10)$$

Since the location of the rust spot is difficult to access physically, we used the vertical length of the welding as a comparison to perform an estimation of rust's height. The rust covers the entire weld in the vertical direction and this has been measured to be between 21-22mm. By counting the number of pixels of the welding in the vertical direction, we get 39 pixels, which results in 21.68mm. Comparing this with the calculated rust height, gives an error deviation between 3.24 and -1.52%.

C. Blade Inspection

In the extensive number of flights we have performed, we experienced that the LiDAR has issues detecting narrow surfaces such as wind turbine blade edges. These areas unfortunately, are some of the most critical areas that should be inspect periodically [17], [18]. This is because the leading edges,

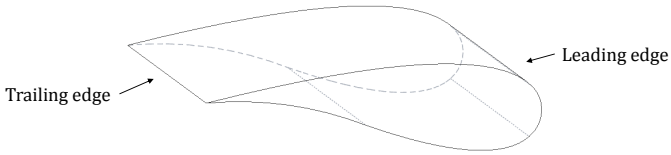

Fig. 8. Cross section of a wind turbine blade.

as sketched in figure 8, at the blade tip are exposed to severe conditions when moving at a high velocity ($\approx 80 ms^{-}1$) and are constantly struck by rain droplets and hailstone impacts at high speed ($100 ms^{-}1$). This produces a large impact force [19], that eventually leads to what is refereed to as leading edge erosion. This will produce over time edge delamination, which is the final stage of the erosion process. One such case is shown in figure 9, where the composite material has degraded due to erosion, and the blade is in a state of delamination.

For the erosion example shown in figure 9, no LiDAR data was available. The data we obtained corresponds to the image shown in figure 10, which is approximately 7 meters below the image in figure 9. The data collected here was a single point measurement at 7.03meters.

This data collection problem is even more acute when trying to measure the trailing edge of the wind turbine blade, due to its sharp features. Figure 11, shows the trailing edge that is approximately 26 meters below the tip of the blade. Applying the LiDAR to this feature and the rest of features up in the blade did not produce any LiDAR measurements.

Fig. 9. Wind turbine's blade tip seen from the leading edge side.

Fig. 10. Leading edge of the wind turbine, approximately 7 from the blade tip.

V. Conclusion

In this paper a Flash Solid-state LiDAR from Leddar was embedded onto a commercial drone, aiming at evaluating the use of such equipment in commercial wind turbine inspections. The goal was to use LiDAR measurements to accurately scaling the images from the camera with the aim of determining its usefulness in detecting the sizes of damages.

The proposed method was used to measure the area of objects of known sizes such as doors and handles that are part of the wind turbine structure. The size of these objects was calculated with an error of 4.60%, 0.17% and -1.75% corresponding to three features, door height, width and handle width.

Next, the size of a rust spot located in a wind turbine's tower was estimated. However, given that the exact size of the rust spot could not be measured due to its inaccessible location in the wind turbine, its size was estimated indirectly from other measurements. Our results show that the rust width could be calculated with a error deviation of 3.24% and -1.52%. From these experiments it can thus be concluded, that our method is well suited to determining with a high degree of accuracy, the size of certain wind turbine tower's features.

Fig. 11. Trailing edge of the wind turbine blade, approximately 26 from the blade tip.

However, our method has some shortcomings. Firstly, it has a relatively low resolution and secondly it was unable to detect objects located at steep angles. This is clearly a problem when a multibeam LiDAR is used to inspect blade tips and its trailing edges sice the Lidar will not be able to measure the distance to these objects. Another problem, that is related to the low resolution of our LiDAR occurs when we try to measure surfaces that are not flat. In this case we used a simple linear approximation of the distance to the points located between the LiDAR beams. However, this approach will not work when applied to more complex shapes.

In our future work we will use a higher resolution LiDAR to address these issues.

Acknowledgment

The Authors would like to thank colleagues Mads Rasmussen and Rene Merrild from Aerodyne AtSite A/S, Denmark, for their support.

References

[1] F. Blaabjerg and K. Ma, "Future on power electronics for wind turbine systems," *IEEE Journal of Emerging and Selected Topics in Power Electronics*, vol. 1, no. 3, pp. 139–152, 2013.

[2] V. Igwemezie, A. Mehmanparast, and A. Kolios, "Current trend in offshore wind energy sector and material requirements for fatigue resistance improvement in large wind turbine support structures–a review," *Renewable and Sustainable Energy Reviews*, vol. 101, pp. 181–196, 2019.

[3] J. P. Jensen, "Evaluating the environmental impacts of recycling wind turbines," *Wind Energy*, vol. 22, no. 2, pp. 316–326, 2019.

[4] L. Wang and Z. Zhang, "Automatic detection of wind turbine blade surface cracks based on uav-taken images," *IEEE Transactions on Industrial Electronics*, vol. 64, no. 9, pp. 7293–7303, 2017.

[5] G. Morgenthal and N. Hallermann, "Quality assessment of unmanned aerial vehicle (uav) based visual inspection of structures," *Advances in Structural Engineering*, vol. 17, no. 3, pp. 289–302, 2014.

[6] P. Durdevic, D. Ortiz-Arroyo, S. Li, and Z. Yang, "Vision aided navigation of a quad-rotor for autonomous wind-farm inspection." Elsevier, 2019.

[7] E. Jasinien, R. Raiutis, A. Voleiis, A. Vladiauskas, D. Mitchard, M. Amos *et al.*, "Ndt of wind turbine blades using adapted ultrasonic and radiographic techniques," *Insight-Non-Destructive Testing and Condition Monitoring*, vol. 51, no. 9, pp. 477–483, 2009.

[8] C. Galleguillos, A. Zorrilla, A. Jimenez, L. Diaz, Á. Montiano, M. Barroso, A. Viguria, and F. Lasagni, "Thermographic non-destructive inspection of wind turbine blades using unmanned aerial systems," *Plastics, Rubber and Composites*, vol. 44, no. 3, pp. 98–103, 2015.

[9] B. E. Schäfer, D. Picchi, T. Engelhardt, and D. Abel, "Multicopter unmanned aerial vehicle for automated inspection of wind turbines," in *2016 24th Mediterranean Conference on Control and Automation (MED)*. IEEE, 2016, pp. 244–249.

[10] A. Gneeniss, J. Mills, and P. Miller, "In-flight photogrammetric camera calibration and validation via complementary lidar," *ISPRS journal of photogrammetry and remote sensing*, vol. 100, pp. 3–13, 2015.

[11] L. D. Jie Chen, "Detection of fault structures with airborne lidar point-cloud data," in *Proc. SPIE 9669, Remote Sensing of the Environment: 19th National Symposium on Remote Sensing of China*, vol. 9669, 2015.

[12] F. Shahdib, M. W. U. Bhuiyan, M. K. Hasan, and H. Mahmud, "Obstacle detection and object size measurement for autonomous mobile robot using sensor," *International Journal of Computer Applications*, vol. 66, no. 9, 2013.

[13] LEDDAR, "Leddar Vu8, 8 segment Solid-State LiDAR Sensor Module," https://leddartech.com/lidar/leddar-vu8-solid-state-lidar-sensor-module/, 2019, online; accessed 17 June 2019.

[14] S. Thrun, W. Burgard, and D. Fox, *Probabilistic robotics*. MIT press, 2005.

[15] R. Siegwart, I. R. Nourbakhsh, and D. Scaramuzza, *Introduction to autonomous mobile robots*. MIT press, 2011.

[16] R. Gonzales, R. Woods, and S. Eddine, "Digital image processing using matlab,(2" ed.)," 2009.

[17] A. Sareen, C. A. Sapre, and M. S. Selig, "Effects of leading edge erosion on wind turbine blade performance," *Wind Energy*, vol. 17, no. 10, pp. 1531–1542, 2014.

[18] H. Slot, E. Gelinck, C. Rentrop, and E. Van Der Heide, "Leading edge erosion of coated wind turbine blades: Review of coating life models," *Renewable Energy*, vol. 80, pp. 837–848, 2015.

[19] M. H. Keegan, D. Nash, and M. Stack, "On erosion issues associated with the leading edge of wind turbine blades," *Journal of Physics D: Applied Physics*, vol. 46, no. 38, p. 383001, 2013.